



A Molecular Chemodosimeter to Probe "Closed Shell" Ions in Kidney Cells

Journal:	<i>Organic & Biomolecular Chemistry</i>
Manuscript ID	OB-ART-09-2023-001408.R1
Article Type:	Paper
Date Submitted by the Author:	31-Oct-2023
Complete List of Authors:	<p>Assel, Amine; University of Monastir Stanley, Meagan ; The University of Southern Mississippi, Chemistry and Biochemistry Mia, Rashid; The University of Southern Mississippi, Chemistry and Biochemistry; Stephen F Austin State University, Chemistry and Biochemistry Boulil, Besma ; Univerisity of Southern Mississippi, Department of Biological Sciences Cragg, Peter; University of Brighton, School of Applied Sciences Owolabi, Iyanuoluwani; Univerisity of Southern Mississippi, Department of Biological Sciences Hetrick, Meredith ; The University of Southern Mississippi, Chemistry and Biochemistry Flynt, Alex; Univerisity of Southern Mississippi, Department of Biological Sciences Wallace, Karl; The University of Southern Mississippi, Chemistry and Biochemistry Ben Jannet, Hichem; University of Monastir Faculty of Sciences of Monastir,</p>

ARTICLE

A Molecular Chemodosimeter to Probe “Closed Shell” Ions in Kidney Cells

Amine Assel^a, Meagan Stanley^b, Rashid Mia^{b&c}, Bisma Boulila^a, Peter J. Cragg^d, Iyanuoluwani Owolabie^e, Meredith Hetrick^e, Alex Flynt^e, Karl J Wallace^{b*} and Hichem Ben Jannet^a

Received 00th January 20xx,
Accepted 00th January 20xx

DOI: 10.1039/x0xx00000x

Two quinidine-functionalized coumarin molecular probes have been synthesized and have been found to bind metal cations (Cd^{2+} , Co^{2+} , Cu^{2+} , Fe^{2+} , Hg^{2+} , Ni^{2+} , and Zn^{2+}) with high affinity in organic-aqueous media (DMSO-HEPES). The chemodosimeters coordinate with the Zn^{2+} ions in a two-to-one ratio (molecular probe: Zn^{2+}) with a $\log \beta$ of 10.0 M^{-2} . Upon the addition of the closed-shell metal ions studied, a fluorescence turn-on *via* an excimer formation is seen at 542 nm due to the quinaldine moiety adopting a *syn* arrangement when coordinated to the metal Zn^{2+} ions. Confocal microscopy monitored free Zn^{2+} ions in the Human Embryonic Kidney cell line HEK293 by coordinating with the chemodosimeter.

Introduction

Designing chemosensors, a molecular system that recognizes other molecules and responds to their presence with a macroscopic change in their electronic properties, is a continuing endeavor. These chemosensors, whether chromogenic or fluorogenic, fall into two broad categories: those involving *reversible* interactions for analyte detection known as chemoreactants whereas chemodosimeters react covalently in an *irreversible* manner with their targets to form a new species with different electronic properties than the original molecule (e.g. colorimetric or fluorometric signature).¹ Molecules based on the chemodosimeter recognition produce high selectivity towards their targets by coupling with chemical events for response amplification.² This approach has immediate applications for analytical purposes,³ but it has also proven fruitful further afield, e.g., in the development of novel stimuli-responsive materials.⁴

One approach to preparing chemodosimeters is to utilize coordination chemistry, a fundamental aspect of chemistry that

impacts every sub-discipline and is omnipresent in the sensing community. Common chelating groups often contain oxygen and nitrogen atoms; for example, amides,⁵⁻⁷ hydrazones,^{8,9} and enamines¹⁰⁻¹² have all been incorporated into molecular chemodosimeters, whereby the recognition event occurs upon the binding of the metal ions. A class of organic molecules that have gained attention for this purpose are poly-heterocycles, where the presence of two or more heterocyclic pharmacophores linked and/or fused within the same organic framework can potentially improve the metal ions molecular recognition.^{13, 14} Moreover, heterocyclic compounds that contain well-known scaffolds, such as a coumarin backbone, a pyrazole group, or triazole moieties, have been shown to have biological, pharmaceutical and medicinal chemistry applications, as they are uncharged compounds with low cytotoxicity.¹⁵ Encouraged by this work, we were prompted to explore versatile possibilities of access to novel hybrid conjugates incorporating coumarin and oxyquinolinyl groups *via* an ethylidene-acetohydrazide linker within the same molecular target, namely the (*E*)-*N*'-(1-(4-hydroxy-2-oxo-2H-chromen-3-yl)ethylidene)-2-(**X**)acetohydrazide in which **X** is quinoline-8-yloxy (**QHC1**) or 2-methylquinolin-8-yloxy (**QHC2**).

The choice of signal transduction mechanism is also critical to the success of chemical sensing paradigms. The utilization of certain functional groups, for example, Schiff bases, amines, and amides, can hinder the fluorescence intensity (i.e., quench) of a molecular fluorophore before binding to the metal ion. Upon the coordination of a metal ion, a hyperchromic shift in fluorescence intensity is observed with closed-shell metal ions, a fluorescence mechanism known as the chelation-enhanced fluorescence (CHEF) mechanism.^{16, 17} The quinoline functional group is also an attractive moiety to include in the molecular probe design as quinoline derivatives are naturally highly fluorescent.^{14, 18, 19} Moreover, the nitrogen atom in the quinolone group can act as an additional coordination site to

^a Laboratory of Heterocyclic Chemistry, Natural Products and Reactivity (LR11E539), Team: Medicinal Chemistry and Natural Products, Faculty of Science of Monastir, University of Monastir, Avenue of Environment, 5019 Monastir, Tunisia.

^b Department of Chemistry and Biochemistry, School of Mathematics and Natural Science, The University of Southern Mississippi, 118 College Drive, Hattiesburg, MS 39406, USA

^c Department of Chemistry and Biochemistry, Stephen F Austin State University, P.O. Box 13006 SFA Station, Nacogdoches, TX 75962, USA.

^d School of Applied Chemical Sciences, University of Brighton, Brighton, BN2 4GJ, UK.

^e Department of Cellular and Molecular Biology, The University of Southern Mississippi, 118 College Drive, Hattiesburg, MS 39406, USA.

^f † Footnotes relating to the title and/or authors should appear here.

^g Electronic Supplementary Information (ESI) available: [details of any supplementary information available should be included here]. See DOI: 10.1039/x0xx00000x

the metal ions, which will influence the electronic properties of the molecular probe.

The metal ion of interest in this study is Zn^{2+} , as it is a closed shell system. Maintaining zinc homeostasis in the human body is of great importance, as Zn^{2+} ions play many biological roles, including the function and pathology of the brain and immune system,²⁰⁻²² mammalian reproduction,²³ and gene transcription^{24, 25} as such, alterations in Zn^{2+} homeostasis has been linked to Alzheimer's disease²⁶, diabetes,²⁷ epilepsy,²⁸ and cerebral ischemia.²⁹ The nature of the function of Zn^{2+} ions for both intra- and intercellular communication requires transitory Zn^{2+} ions; however, it proves difficult to differentiate between protein-bound Zn^{2+} and free Zn^{2+} ions experimentally.³⁰ To understand the messaging properties of Zn^{2+} ions, it is crucial to determine their concentration under steady-state conditions. This quantification can also determine if an excess or deficiency in Zn^{2+} ions is present and how these homeostatic fluctuations result in various pathophysiology's. One of the most common techniques for detecting free Zn^{2+} is the use of low molecular weight fluorescent chelating agents, for example the Zinspy sensors used by Lippard.^{31, 32}

An extensive library of fluorescent probes for Zn^{2+} ions exist, however few detect Zn^{2+} in biological systems, which require specific considerations, such as pH, as metals are acidic and will form insoluble hydroxides in water without a buffer present. While Zn^{2+} ions have one of the highest affinities for ligands (particularly N-containing ligands), according to the Irving-Williams series,³³ cellular concentration of metal ions can vary greatly, so the presence of less competitive metal ions may need to be adjusted for. Concentrations of Zn^{2+} ions also vary depending on the location in the body, which can range from picomolar (pM) concentrations in the cytosol to millimolar (mM) range in the vesicles.^{34, 35} Moreover, metal and pH buffering and buffering capacity must be considered when applying sensing technology in cells, as some probes' fluorescent properties and responses are pH dependent. Extensive consideration of these parameters must be taken into account, so that the chosen probe design that utilizes the previously mentioned structures and detection mechanisms provides a high sensitivity, specificity, and selectivity that reflect the appropriate cellular requirements.

Here we report two chemodosimeters containing the elements within a single molecule to detect closed-shell metal ions in an aqueous system. As these types of poly-heterocycles have been shown to work in biological media, we have shown that they can monitor Zn^{2+} ions in aqueous systems as high as 99% HEPES (25 mmol·dm⁻³, pH = 7.4) and in a human embryonic kidney (HEK 293) cell line.

Results and Discussion

Sensor design, synthesis, and characterization

This work aims to understand the photophysical mechanism responsible for the optical response with metal

ions, as their chloride salts in an aqueous environment or acetate salts in organic media. As the hydrazide moiety is a combination of amide and imine functional groups, it will make an excellent candidate to bind metal ions. Due to the hydrazide moiety in **QHC1** and **QHC2**, there are a number of Lewis basic sites capable of coordinating to metal ions via different binding modes, such as a mono-, di-, or tridentate fashion (Fig. 1), and it also provides the preferred molecular geometry that the metal ion will adopt under experimental conditions. Previously, our group has shown that the anion can deprotonate the enol proton that is involved in the Resonance-Assisted Hydrogen Bonding interaction (RAHB) to form the bidentate binding motif ($N^{\wedge}O^-$), which drastically changed the optical response upon the addition of metal acetate salts in DMSO, by inhibiting the ESIPT mechanism and producing a CHEF signal upon the binding of metal ions.¹⁰

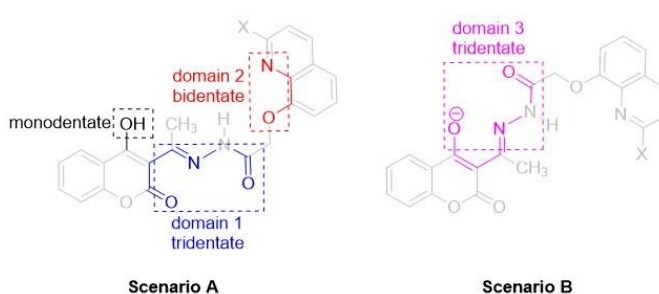


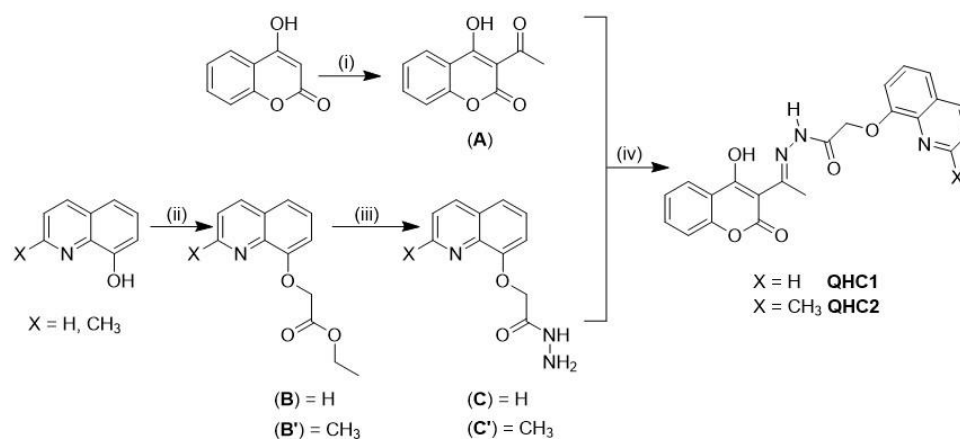
Fig 1. Three possible binding domains and coordination modes for metal binding to **QHC1** (X = H) and **QHC2** (X = methyl) molecular probes.

Synthesis

The molecular probes **QHC1** and **QHC2** were synthesized in four steps (Scheme 1). The coumarin portion of the chemodosimeter was prepared by reacting the commercially available 4-hydroxycoumarin with acetic anhydride to form 3-acetyl-4-hydroxycoumarin (intermediate A) in excellent yields (94%). The two acetohydrazide quinolone derivatives (intermediate C (X = H) and C' (X = CH₃)) were prepared in the same way. Either the commercially available 8-hydroxyquinoline or 8-hydroxyquinaldine were reacted with ethylchloroacetate to form the ether derivatives (intermediate B or B'). These were then subsequently reacted with hydrazide hydrate to form the acetohydrazide derivatives. The coupling of 3-acetyl-4-hydroxycoumarin with the acetohydrazide with a catalytic amount of glacial acetic acid (a few drops) produced the desired compounds in good yields (>75%). Interestingly, only a single stereoisomer was seen NMR in DMSO-*d*₆, *vide infra*

Structural Studies

It is known that the hydrazone functional group can have different conformational isomers. Moreover, the RAHB ring between the enol and the hydrazine group can produce enol/*keto* tautomers. It is plausible that different geometries and tautomers might exist in solution, which can complicate the



Scheme 1. Synthesis of **QHC1** and **QHC2** (i) (CH₃CO₂)₂O, C₅H₅N, Δ (ii) ethylchloroacetate, K₂CO₃ DMF, Δ (iii) NH₂NH₂ hydrate, EtOH, RT, (iv) EtOH, Δ.

NMR spectrum.^{36,37} Ligand **QHC2** was extensively studied using one-dimensional (1D) and two-dimensional (2D) NMR spectroscopy (HSQC, HMBC, and ROSEY) in DMSO-*d*₆. The numbering system (Fig. S1) is used to assign the proton and carbon atoms, and the full spectra of 1D and 2D are reported in the supporting information (**QHC1** Figs S2 to S6 and **QHC2** Table S1-assignment and Figs. S7 to S26-spectra). Compound **QHC2** exists as a single stereoisomer, namely the *s-cis*-enol-(*E*) imino-amide conformation. A broad signal is observed at δ_{C} 15.61 ppm assigned to the enol OH group. This signal could have been assigned to the NH signal, but this possibility was ruled out as hydrazide NH groups typically do not appear beyond δ_{H} 12.5 ppm in DMSO-*d*₆,³⁸ furthermore the oxygen atom is more electronegative, thus the protons acidity will cause it to appear further downfield. The HMBC spectrum, using the ¹³C attached proton (APT) spectra correlated with the ¹H NMR, was very informative in assigning all of the quaternary carbon atoms in the ligand's *s-cis*-enol-(*E*) imino-amide conformation (Figs. S19 to S24). The enol carbon (4-OH) is shifted the furthest downfield and is seen at δ_{C} 178.9 ppm. Carbon-3 and carbon-9 are observed at δ_{C} 95.4 and δ_{C} 172.1 ppm, respectively. These carbon chemical shifts are in excellent agreement with the resonances of carbon atoms in enols and imines. Finally, the carbon atom on the amido functional group (C-11) is seen at δ_{C} 166.6 ppm, typically indicative of a carbon chemical shift seen for amides. These chemical shifts suggest that the hydrazone moiety is locked in as the *E* isomer. However, the quinoline functional moiety seems to be freely rotating around the amide group in the solution, as shown by the two ROESY strong nOes between both the methyl (H-10) and the methylene (H-12) protons and the aromatic proton (H-19) of the quinoline group are seen. This phenomenon can only occur if these functional groups come into proximity to each other (Figs. S25 and S26).

NMR Studies

To obtain an understanding of the coordination environment, we prepared either one-to-one or two-to-one ratio solutions of

the molecular probe and Zn(CH₃CO₂)₂ *in situ*, and ran the 2D experiments. However, it was found that a precipitate formed during the time data was acquired, reducing the concentration of the complex in solution, thereby rendering it challenging to obtain a reasonable ¹³C NMR spectrum to be used in the 2D NMR experiments. Attempts were made to keep the solid in solution at an elevated temperature (358 K) but failed. However, the ¹H NMR provided enough information to plausibly predict the geometry around the metal centre, supported by molecular modelling calculations (*vide infra*).

Two solutions of **QHC1** (20 mmol·dm⁻³ in DMSO-*d*₆) were prepared. One solution was mixed in a one-to-one ratio and the other a two-to-one ratio of the probe and Zn(CH₃CO₂)₂ salt. The ¹H NMR spectra were recorded within a few minutes of preparation. Within this short timeframe, several species could be observed. The signals assigned to the protons attached to the quinoline and coumarin groups have significant overlap and complex splitting patterns, rendering the exact assignment difficult without obtaining the 2D spectra (Figs. S27 and S28). However, the region between δ_{H} 4.6 and 5.8 ppm was informative and helped us understand the possible coordination environment. The methylene protons (H-12) (see NMR numbering system in the ESI, Fig. S1) are seen as a singlet at δ_{H} 5.07 ppm for **QHC1**. Upon adding one equivalent of Zn(CH₃CO₂)₂, two distinctive sets of signals are observed (Fig. 2A). The first set of H-12 geminal protons appears as two characteristic diastereotopic protons at δ_{H} 5.26 and 5.55 ppm with a strong second-order splitting effect and a coupling constant of $J = 12.8$ Hz, typical of a ²*J* coupling. Additionally, another singlet is seen at δ_{H} 4.84 ppm, which has shifted upfield by δ_{H} 0.23 ppm. These two chemical environments suggest that two species are present. As the sample was prepared in a one-to-one ratio, it is reasonable to assume that the Zn²⁺ ion can coordinate to different domains of the molecular probe (Fig. 1). It is unlikely that a coordination number six (CN6) would be possible with **QHC1**, due to a significant amount of ring strain that will occur. It is likely that a CN4 (tetrahedral) geometry occurs, resulting in a tridentate binding motif (Fig 1, domain three) with the remaining coordination site occupied by either

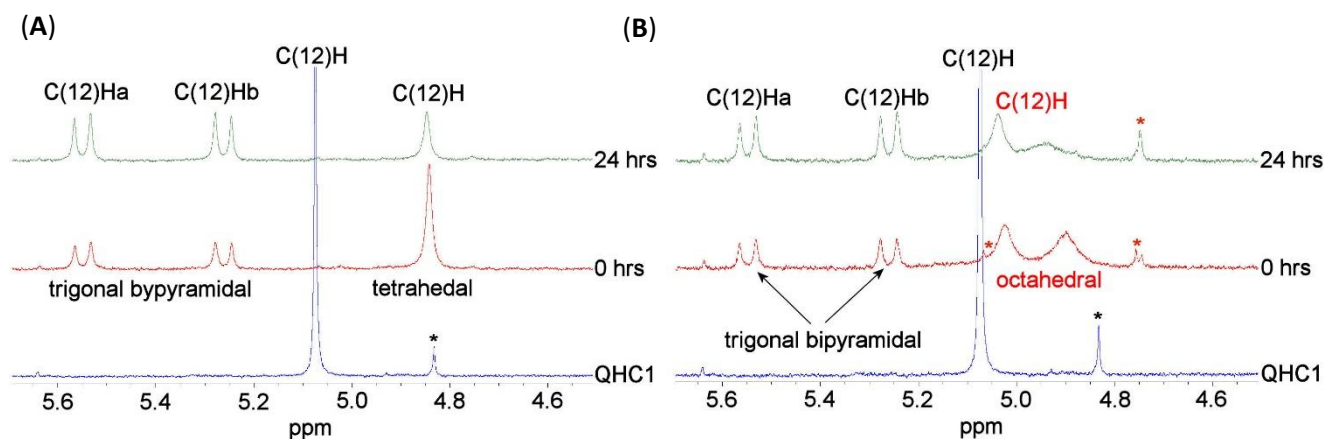
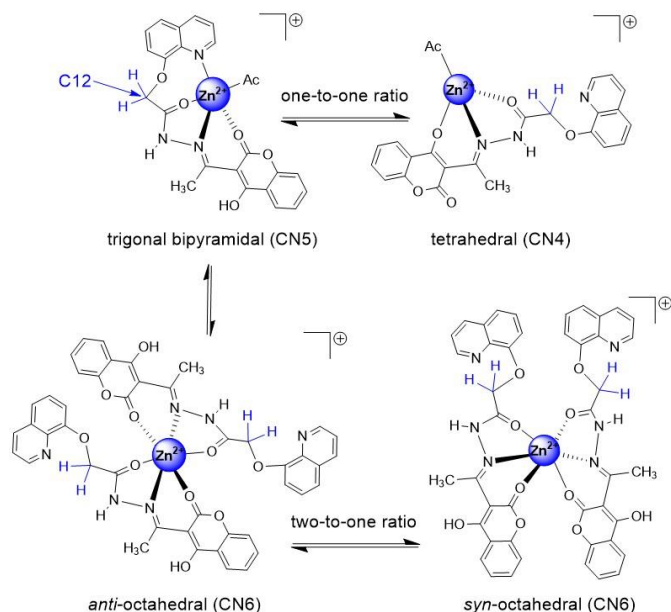


Fig. 2. Expansion of the ^1H NMR spectrum ($\text{DMSO-}d_6$, 298 K) of the methylene region, showing the signals arising from the different geometries observed in situ, whereby **QHC1** and $\text{Zn}(\text{CH}_3\text{CO}_2)_2$ were mixed in a one-to-one (A) and two-to-one (B) ratio

solvent or one of the counter ions. A CN5 (trigonal bipyramidal-*tbp*) would also be a reasonable geometry whereby both domain one and domain two are coordinated to the zinc centre. The free rotation around C-12 must be hindered to obtain geminal coupling. This can only be achieved if the nitrogen atom on the quinoline moiety is coordinated to the Zn^{2+} ion, producing a scenario whereby CN5 is achieved. If the nitrogen atom is not partaking in coordination and only forming a complex *via* a tridentate fashion, it would leave the protons to freely rotate and be indistinguishable on the NMR time scale. To see if one geometry has a preference, we monitored the ^1H NMR over 48 hours. Over that time, the integration of the peaks stayed consistent, suggesting that the two geometries are in equilibrium in $\text{DMSO-}d_6$.

As zinc complexes are commonly found in an octahedral geometry, it is reasonable to assume that the octahedral geometry can exist in solution. Thus, the NMR investigation was repeated with the ratio between **QHC1** and $\text{Zn}(\text{CH}_3\text{CO}_2)_2$ changed to two-to-one. Different chemical shifts were seen for

the methylene protons, suggesting that a different species is present in the solution (Fig. 2B). Interestingly, the CN5 structure is present too, as the exact chemical shifts at δ_{H} 5.26 and 5.55 ppm are present, assigned to C(12)H. However, another set of signals appears at δ_{H} 4.90 and 5.02 ppm and a set of diastereotopic signals have shifted up-field. Both the molecular probes can coordinate to the Zn^{2+} ion in an *anti* and *syn* orientation, with respect to the quinoline groups (Scheme 2). When $\text{Zn}(\text{CH}_3\text{CO}_2)_2$ was added to **QHC2** in a one-to-one ratio, the ^1H -NMR spectrum was significantly different, which was much easier to assign and identify a single tetrahedral species in solution. This is a consequence of steric hindrance as the methyl group that is *ortho* to the nitrogen atom on the quinoline moiety is bulky enough to prevent any interaction with the metal ion and only a single tetrahedral species is seen after three hours (Fig. S28). As **QHC1** showed different species in solution, this would undoubtedly complicate any titration investigations. Therefore, only **QHC2** was used to determine the metal binding ability with Zn^{2+} ions. The ^1H -NMR titration was carried out in $\text{DMSO-}d_6$ at room temperature. Molecular probe **QHC2** is an extremely effective ionophore with a binding affinity for Zn^{2+} ions too high to measure in $\text{DMSO-}d_6$ at 20 $\text{mmol}\cdot\text{dm}^{-3}$. However, the NMR titrations were very useful in aiding our understanding of the species that are present in the solution. Upon 0.1 equivalent additions (up to half an equivalent), the aromatic signals from the quinoline and coumarin broaden significantly. The methylene signal seen at 5.04 ppm splits into two distinctive signals (Fig. S29 and S30), and the methyl protons assigned to C(21H) move up-field direction by 0.02 ppm. A plausible explanation for these chemical shifts is that the metal is bound in a two-to-one ratio in a *syn*-octahedral geometry and the shift is a consequence of the shielding between the methyl protons that are in close proximity to the ring current of the quinoline group on an adjacent **QHC2** molecule (see modelling section). Continuous additions of Zn^{2+} ions significantly sharpen the NMR spectra, which are highly symmetrical, suggesting that only a single species is in solution. Once the one-to-one ratio is reached and there are no other changes up to the addition of three equivalents of $\text{Zn}(\text{CH}_3\text{CO}_2)_2$ (Fig. 3). This supports the notion that at the lower



Scheme 2. Proposed geometries based on the chemical shift and splitting patterns seen for the geminal methylene protons C(12)H (highlighted in blue).

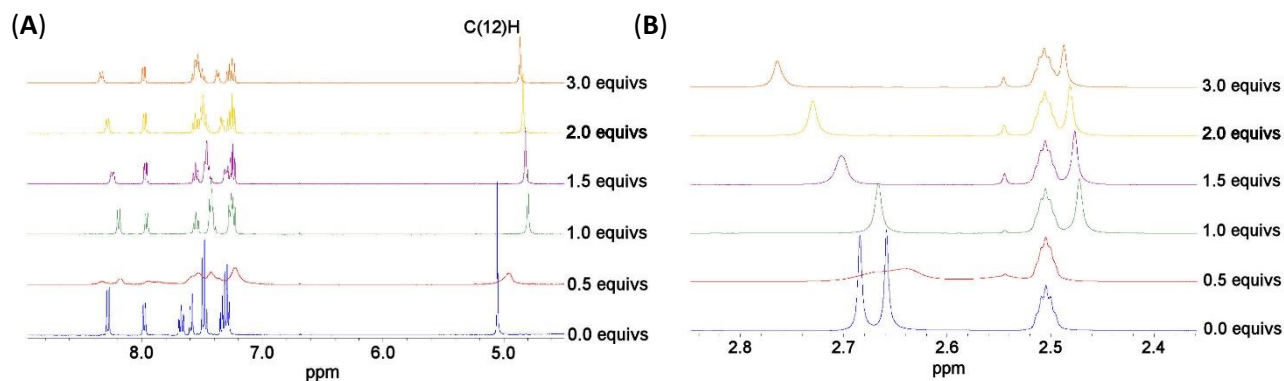


Fig. 3. ^1H NMR titration, addition of Zn^{2+} ions ($20 \text{ mmol}\cdot\text{dm}^{-3}$, $\text{DMSO}-d_6$, 298 K). Full titration plots are shown in the ESI. (a) aromatic region and (b) methyl region.

concentrations, the Zn^{2+} ion is bound in a two-to-one ratio (octahedral), but as more metal is bound, there is an interconversion with the species to a tetrahedral environment.

To support the NMR work, an ESI-MS experiment was carried out by preparing a one-to-one solution by adding the appropriate volumes of **QHC2** and $\text{Zn}(\text{CH}_3\text{CO}_2)_2$ stock solutions in a 1.0 mL volumetric flask to make a $50 \text{ mmol}\cdot\text{dm}^{-3}$ solution, after which $100 \mu\text{L}$ of this solution was diluted with $900 \mu\text{L}$ acetonitrile. The MS spectrum, which was recorded in both negative and positive mode, is very different for free **QHC2** and the coordinating complex. The free probe ran in the positive mode shows an m/z value of 418.1 representing $[\text{QHC2}+\text{H}]^+$, interestingly a number of dimer species are also observed at m/z 835.2, 858.8 and 889.0, assigned to $[2\cdot(\text{QHC2})+\text{H}]^+$, $[2\cdot(\text{QHC2})+\text{Na}]^+$ and $[2\cdot(\text{QHC2})+3\text{H}_2\text{O}+\text{Na}]^+$, respectively (schemes S1 and S2 and Fig. S31). In the mass spectrum of **QHC2** upon the addition of $\text{Zn}(\text{CH}_3\text{CO}_2)$ (one-to-one), two distinct Zn^{2+} (double-charged) species are seen at m/z 279.0 and 358.0 assigned to two solvated species, $[\text{Zn}(\text{QHC2})\cdot 2\text{H}_2\text{O}\cdot\text{CH}_3\text{CN}]^{2+}$ and $[\text{Zn}(\text{QHC2})\cdot 2\text{H}_2\text{O}\cdot 3\text{CH}_3\text{CN}\cdot\text{DMSO}]^{2+}$ (Fig S33B). The base peak is seen at $m/z = 467.1$ assigned to $[\text{Zn}(\text{QHC2})_2\cdot 2\text{H}_2\text{O}]^{2+}$ two-to-one, species (Fig. S33). Interestingly in the negative mode, only the one-to-one species was seen, whereby $[\text{Zn}(\text{QHC1})(\text{CH}_3\text{CO}_2)\cdot\text{H}]^-$ is observed at $m/z = 525.0$, (Fig. S32). Both the gas phase work and the solution studies are in excellent agreement and supports the speciation of the metal species.

Several attempts were made to grow X-ray-quality crystals with no success. One plausible reason could be due to the speciation of different coordination compounds, rendering it difficult for one of the species to crystallize into its most thermodynamically structure (see modelling section).

Optical Studies

Absorbance, Steady-State, and Lifetime Fluorescence Studies in Organic Media

Both molecular probes have a three membered ring system, two fused and another formed by the RAHB system; therefore,

the conjugation will push the absorbance into the visible region. Upon the binding of metal ions, the spectroscopic properties will be significantly affected, producing absorbance shifts by redistributing the electronic density upon the coordination of metal ions in the different binding domains in the molecular probe. We investigated the ion-pair effect (acetate and chloride ions) on our imine-enamine-based hydroxycoumarin probes (**QHC1** and **QHC2**), which are also tethered to quinoline groups (Scheme 1). Initially, the studies were carried out in DMSO which produces a mundane spectroscopic signature compared to other organic solvents that can drastically affect the spectrum due to solvatochromism. Moreover, the acetate ion was initially used as the counter ion as we have previously shown that the metal acetate could deprotonate the OH group on the enol to form the chelating motif to coordinate with the metal ions.¹⁰ The initial UV-Vis band is seen at 331 nm for **QHC2**, assigned to the $n\text{-}\pi^*$ transition (the $\pi\text{-}\pi^*$ band is seen at 261 nm), with a calculated molar absorbance coefficient of $13,909 \text{ mol}\cdot\text{dm}^{-3}\cdot\text{cm}^{-1}$ (Fig. S34). After adding the metal ions (as their acetate salts), a bathochromic shift was observed through an isosbestic point for all the metals investigated (ESI Figs S35 to S39). Significant wavelength changes occurred when aliquots of different metal acetate salts (Cd^{2+} , Co^{2+} , Cu^{2+} , Fe^{2+} , Hg^{2+} , Ni^{2+} , and Zn^{2+} ions), were added to a $50 \mu\text{mol}\cdot\text{dm}^{-3}$ solution of the molecular probes in DMSO. The changes in the absorbance spectra allowed us to calculate the binding affinity between the probes (for which **QHC2** provides a representative example) and metal ions by using a nonlinear model fit (see ESI for details). Interestingly, all metal ions show a very strong two-to-one (probe-to-metal) binding except Hg^{2+} , which fits a K_{11} species (Table 1). The speciation and the formation constants obtained align reasonably with each metal ions most common geometries in their +2-oxidation state. For example, the four transition metal ions (Co^{2+} , Cu^{2+} , Fe^{2+} , and Ni^{2+}) are often found in tetrahedral/square planar or octahedral geometry. The Co^{2+} and Ni^{2+} ions have the same binding constants for K_{11} and K_{21} , suggesting that both the tetrahedral/square planar vs. octahedral geometries are in equilibrium in DMSO. In contrast, the Cu^{2+} and Fe^{2+} seem to favour the K_{21} species, which suggests

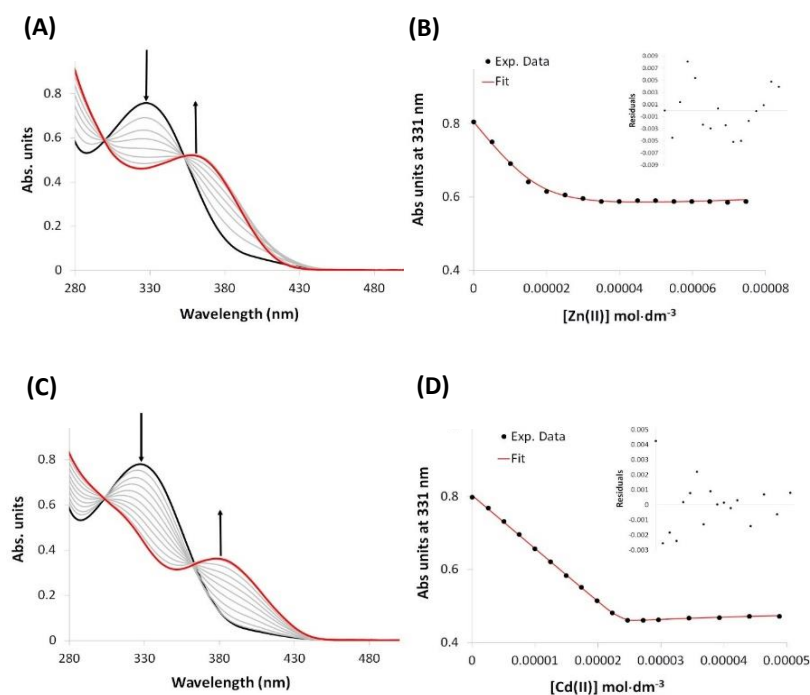


Fig 4. (A) absorbance spectra (B) binding isotherm of **QHC2** upon the addition of increments of $\text{Zn}(\text{CH}_3\text{CO}_2)_2$ and (C) absorbance spectra and (D) binding isotherm of $\text{Cd}(\text{CH}_3\text{CO}_2)_2$ in DMSO; $[\text{QHC2}] = 50 \mu\text{mol}\cdot\text{dm}^{-3}$

that the octahedral species predominates in DMSO, in which the metal coordinates to three binding sites in each molecular probe. A similar trend is seen for the group 12 triad. As all have a d^{10} configuration, there is no spectrochemical preference from the ligand field stabilization effect, thus no preference in geometry. Consequently, tetrahedral, trigonal bipyramidal, and octahedral geometries are found for all three metals. Additionally, it is known that Hg^{2+} is often in a linear geometry due to the available $6s$ orbitals for bonding. The binding affinities for Cd^{2+} and Zn^{2+} ions lie towards the K_{21} species. It is reasonable to have two of the molecular probes coordinating to the metal ion in an octahedral environment. Moreover, Cd^{2+} ions are more often found with a coordination six than Zn^{2+} ions,³⁹ which might suggest why K_{21} for Cd^{2+} is significantly greater than for Zn^{2+} (Table 1). This is also reflected in the shape of the binding isotherms obtained (Fig 4.) where the isotherm for the Cd^{2+} is sharper than that for Zn^{2+} (Fig 4).

Table 1. Formation constants obtained from the coordination of metal²⁺ acetate salts with **QHC2**. Experiments were run in DMSO at 25 °C, isotherms are shown in ESI Figs. S30 to S34).

Metal	Log K_{11} (M^{-1})	Log K_{21} (M^{-1})	Log β (M^{-2})
Co^{2+}	5.66(±16.2%)	5.17(±20.0%)	10.8(±18.0%)
Cd^{2+}	3.32(±40.0%)	9.54(±29.0%)	12.9(±32.7%)
Cu^{2+}	2.71(±10.8%)	5.92(±15.4%)	8.63(±14.0%)
Fe^{2+}	3.66(±14.2%)	5.07(±5.6%)	8.73(±9.20%)
Hg^{2+}	5.64(±23.2%)	-	-
Ni^{2+}	5.04(±17.4%)	5.07(±23.6)	10.1(±20.5%)
Zn^{2+}	3.95(±20.0%)	6.00(±5.8%)	9.95(±11.4%)

Note: K_{21} refers to the formation constant for the species containing two probes molecules per metal ion. The errors are high due to the high binding in DMSO.

Interestingly, when the chloride salts were used, only the one-to-one species was dominant in DMSO and the binding affinity for log K_{11} for **QHC2** upon the addition of ZnCl_2 was determined to be $3.90 (\pm 2.14) \text{ M}^{-1}$ and $4.34 (\pm 1.76)$ for CdCl_2 (Figs. S40 and S41). This suggests that the metal ions are bound in domain one or domain two (Fig. 1) as the chloride anion cannot deprotonate the enol proton.

Another fluorescent phenomenon known to occur in hydroxycoumarin fluorophores that contain an imine-enamine motif is the ESIPT mechanism followed by CHEF when in the presence of closed-shell metal(II) acetate salts.^{10, 40} Both molecular probes described in this work contain the imine-enamine motif. However, as these compounds contain a quinoline group, which is also fluorescent, the emission band will overlap with the *keto** band, which is often weak. Consequently, the emission band attributed to the quinoline moiety masks any ESIPT mechanism in the steady-state spectrum, however, it is clear that the ESIPT process is taking place in these probes, as the fluorescence lifetime decay shows significantly different decays (*vide infra*). Interesting emission signatures were observed upon adding $\text{Zn}(\text{CH}_3\text{CO}_2)_2$ salts, which differ from those of chloride salts. We have previously shown that an excimer formation is observed upon adding metal ions, referred to as anion-induced-self-assembled process.⁴¹ As the absorbance data suggested, a two-to-one probe-to-metal seems to be the most likely when the acetate salt was used and a one-to-one species when the chloride ion was investigated in DMSO. Therefore, the emission spectra should inform our understanding of the coordination environment, depending on the fluorescence signature. One plausible emission signature would be the observation of an excimer band when two quinoline groups are in close proximity which can occur inter or

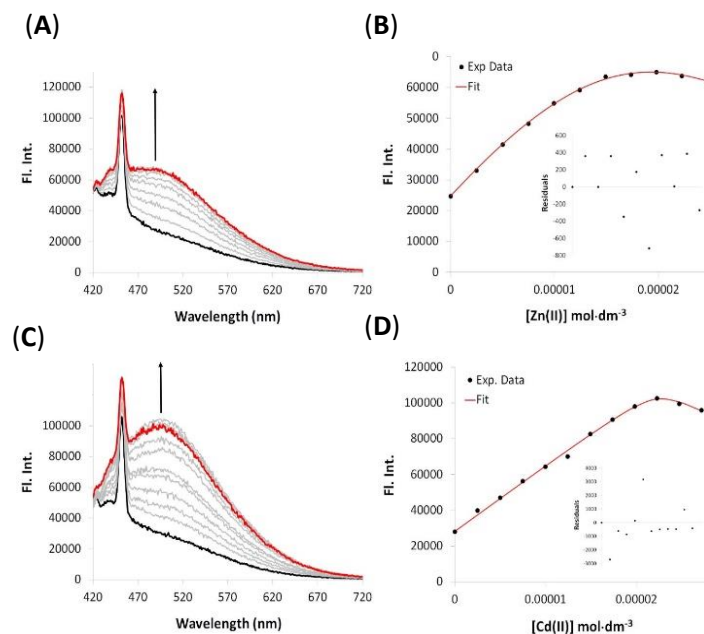


Fig 5.(A) Emission spectra ($\lambda_{\text{ex}} = 400 \text{ nm}$) (B) binding isotherm of **QHC2** upon the addition of increments of $\text{Zn}(\text{CH}_3\text{CO}_2)_2$ and (C) Emission spectra ($\lambda_{\text{ex}} = 400 \text{ nm}$) and (D) binding isotherm of $\text{Cd}(\text{CH}_3\text{CO}_2)_2$ in DMSO; $[\text{QHC2}] = 50 \mu\text{mol}\cdot\text{dm}^{-3}$.

intramolecularly. The intermolecular excimer is ruled out due to the initial concentration being low. **QHC1** and **QHC2** show monomer emission bands at 361 and 390 nm ($\lambda_{\text{ex}} 350 \text{ nm}$), assigned to the $S_0 \leftarrow S_1$ transitions on the monomer. Upon the addition of $\text{Zn}(\text{CH}_3\text{CO}_2)_2$ and $\text{Cd}(\text{CH}_3\text{CO}_2)_2$ a broad and featureless band started to appear at 501 nm, which plateaus out at half equivalent of metal salt; further additions decreased the excimer band (Fig. 5). The binding affinity at the lower concentrations could be modelled using the K_{21} models that were used for the absorbance data, whereby $\log K_{11}$ and $\log K_{21}$ were calculated to be 4.97 ($\pm 21.0\%$) and 5.12 ($\pm 1.66\%$), respectively ($\beta = 10.1$ ($\pm 11.2\%$)) for Zn^{2+} and $\log K_{11}$ and $\log K_{21}$ found to be 3.14 ($\pm 85.0\%$) and 8.97 ($\pm 34.0\%$), $\beta = 13.1$ (44.7%) respectively.

The emission spectrum of **QHC1** in DMSO shows transitions at 420 and 443 nm together with a broad band centered around 542 nm. The former two wavelengths can be assigned to the 8-hydroxy quinoline moiety.⁴² In contrast, the latter band at 542 nm indicates a proton transfer process characteristic of the ESIPT mechanism *via* an enol-*keto* tautomerization. Compound **QHC1** follows a triexponential decay, where τ_1 , τ_2 and τ_3 is calculated to be 5.2(6), 20.8(8) and 1.5(1) ns, respectively (Fig S42, Table S2). The first decay rate (τ_1) makes up approximately 37% of the relative amplitude, and τ_2 and τ_3 contribute 56% and 7%, respectively (Table S2). It is impossible to identify the particular decay constants for each species in the solution. However, it is reasonable to assume that the three decay rate constants are a consequence of enol-*keto* tautomerization and isomerization, which is based on the extensive work published on the well-known HBO/HBS systems, (Fig S43).⁴³⁻⁴⁵ Upon the addition of $\text{Zn}(\text{CH}_3\text{CO}_2)_2$ in a two-to-one ratio the decay profile is fitted to a triexponential, indicative of multiple species in solution, in excellent agreement with the NMR studies. The

decay for τ_1 (5.2(6) ns) is very similar to the free probe, but significant changes in τ_2 and τ_3 are seen with values of 12.2(5) and 7.0(3) ns, respectively ($\lambda_{\text{ex}} 400 \text{ nm}$). The steady-state emission spectrum shows an enhancement, a more fluorescent species, therefore a slower decay profile would be expected.

Absorbance and Steady-state and life-time Fluorescence Studies in Aqueous media

To use these dyes in biological environments it is important to investigate their potential in aqueous systems at a controlled pH. Protonation of the quinoline functional group produces significant perturbations in its electronic structure⁴⁶ resulting in drastic changes in the fluorescence spectrum. Before we investigated the optical response between the ligand and various metal ions in an aqueous solution, we investigated the behaviour of **QHC2** with tetrafluoroacetic acid (TFA). Addition of TFA in an aqueous-DMSO systems showed a very broad band at 525 nm ($\lambda_{\text{ex}} 350 \text{ nm}$) when the spectrum was acquired within a few minutes of making the sample (Fig. S44 and S45). When the quinoline functional group is protonated it can result in self-aggregation and intermolecular excimer formation can occur. This is supported by the gas phase MS experiments in which dimers are observed. Over 24 h this band drastically decreases in intensity, presumably to the repulsion of the positive charge that breaks up the aggregation, due to electrostatics (Figs S44 and S45), but when the pH was controlled at 7.4 this band was not seen. Therefore, HEPES (25 mmol·dm⁻³, pH 7.4) was used in the following aqueous studies.

Dimethyl sulfoxide is a highly competitive solvent and can hinder the binding of metal ions to molecular probes as it is known to be a coordinating solvent. However, the surprisingly

high binding constants between **QHC1** and **QHC2** discussed in the previous section suggests that the solvent is not affecting the molecular probes' abilities to coordinate metal ions in any meaningful way. Moreover, organic solvents are not conducive for biological or environmental imaging applications, as sensing in those fields often require water soluble probes. Many cells can tolerate a certain percentage of organic solvent,⁴⁷ but it would be beneficial to work in an aqueous environment. There are many reports claiming that a particular system works in aqueous solution, but a certain amount of organic solvent is usually needed, often to dissolve the molecular probe. Additionally, the role of the acetate ion is a little controversial and complicated in biological conditions, it is believed to be beneficial for certain diseases and disorders, yet it has also been linked to a major contributor to cancers. Conversely, the chloride ion has a physiological significance and plays vital roles in the regulation of osmotic pressure, electrolyte balance and acid-base homeostasis.⁴⁸ The chloride ion exists in all body fluids and is the most abundant extracellular anion. Therefore, we switched the metal salt to the chloride ion and only investigated the two closed-shell metal ions (Zn^{2+} and Cd^{2+}) in our aqueous studies. The UV-vis studies were undertaken in four different HEPES:DMSO solvent system (25 mmol·dm⁻³ HEPES; pH 7.4). Solutions (50 μmol·dm⁻³) of both **QHC1** and **QHC2** were prepared in the following ratios (100% DMSO; 50% DMSO:50% HEPES; 25% DMSO:75% HEPES and 5% DMSO: 95% HEPES). Aliquots of $ZnCl_2$ were added, the binding isotherms and binding constants are shown in Fig 6 and Table 2, respectively (Figs S46 to S51). The binding constants are lower in the aqueous solution than 100% DMSO which is not surprising as water is a highly competitive solvent that will compete to coordinate the metal ion. Once the percentage of water was greater than 50%, two species existed in solution, presumably the equilibrium between the tetrahedral vs octahedral geometry.

Table 2. Formation constants obtained from the coordination of metal (M^{2+}) chloride salts with **QHC2**. Experiments were run in different aqueous-DMSO ratios at 25 °C.

	Zn ²⁺			Cd ²⁺
	log K_{11} (M-1)	log K_{21} (M-1)	log β (M-2)	log K_{11} (M-1)
DMSO (100%)	3.90 (±2.14%)	-	-	4.34 (±3.59%)
DMSO:HEPES (50:50)	5.12 (±3.70 %)	-	-	5.01 (±5.15%)
DMSO:HEPES (25:75)	1.72 (±8.68 %)	6.64 (±6.90)	8.36 (±7.27%)	4.47 (±2.38%)
DMSO:HEPES (5:95)	4.57 (±9.22)	4.66 (±10.1%)	9.26 (±9.63)	5.02 (±6.90%)

Fluorescence life-lifetime studies were also carried out in a 50:50 mixture of DMSO:HEPES (25 mmol·dm⁻³; pH 7.4) before and after the addition of $ZnCl_2$. Like the life-time decay for the 100% DMSO solution described above, the decay profile for

QHC1 was fitted to a triexponential, where τ_1 , τ_2 and τ_3 were determined to be 6.6(12), 15.1(14) and 7.4(5) ns, respectively (λ_{ex} 350) nm (Figs. S52, and table S3). Interestingly, the addition of 50% HEPES does not change τ_1 or τ_2 by any appreciable amount, but there is a drastic change in τ_3 . This suggests that τ_3 is a species that is significantly influenced by the water content, which remarkably forms a very short-lived fluorophore. Upon the addition of $ZnCl_2$, the τ_2 seems to stay strikingly constant in comparison to the $Zn(CH_3CO_2)_2$ in DMSO (*vide supra*) This suggests that the fluorescence behavior is influenced by the coordinating anion (acetate vs. chloride). Moreover, τ_1 also stays essentially constant over the titration in the two different solvent system, which insinuates that neither the metal nor anion is responsible for the decay in that species, only the solvent system used.

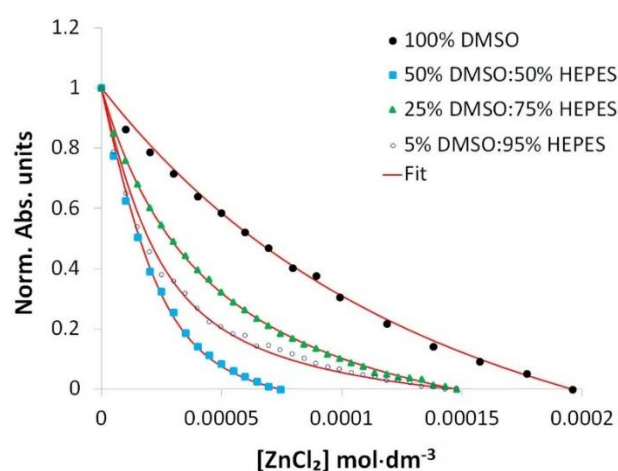


Fig 6. The binding isotherm of $ZnCl_2$ in DMSO:HEPES systems; $[QHC2] = 50 \mu\text{mol}\cdot\text{dm}^{-3}$.

Molecular Modelling Calculations

To support the fluorescence life-time studies of the free molecular probes DFT calculations (DFT/B3LYP/6-31G*) were carried out to investigate the likely stabilities of the ligands and complexes formed for **QHC2**. The free molecular probe can exist as different tautomers and geometrical isomers in solution. Initial calculations were carried out in the gas phase followed by a DMSO and water a continuum. Both the gas phase and DMSO solvent shell converged to the *keto* tautomer being the most thermodynamically stable tautomer whereby the hydrogen atom resides on the nitrogen atom to form the amide moiety. However, the stabilities of the geometric isomers differed in the two phases. The *Z-keto* isomer structure seems to be the most likely in DMSO and the *E-keto* structure in the gas phase. However, when the calculations were carried out using a water continuum, the enol isomer prevails. The calculations suggest that the amide (associated with the hydrazide group) seems to easily tautomerize to form an iminol group, which can be stabilized by hydrogen bonding interactions with water

molecules (Figs. S53 to S55). The DFT calculations suggest that there are a number of thermodynamically favourable conformers, which supports the data obtained in the lifetime studies.

Despite the unrealistic Gibbs free energies obtained for the coordination compounds the simulations clearly indicated a preference for the octahedral *syn* structures over other possible geometries and for the neutral *syn*-[Zn(QHC2)₂] in which the ligand has been deprotonated. Both the NMR and steady state work suggest that the Zn²⁺ ion can adopt different species in solution, suggesting that the Zn²⁺ is very versatile with respect to the number of ligands and coordination sites that can be embraced by the metal center (Fig. S56). The neutral *syn*-[Zn(QHC2)₂] shows that the two ligands are bound to the Zn²⁺ ion in a tridentate fashion in domain one (Fig. S57). The *syn* geometry clearly supports the intra excimer formation, observed in the steady-state spectrum (Fig. 5). Moreover, the two quinoline groups adopt a *trans* orientation where the methyl group from one of the ligands is eclipsed with the ring system of the quinolone group on the second ligand. This is in excellent agreement with the NMR studies, as there is a significant up field shift observed for the methyl protons (see NMR section).

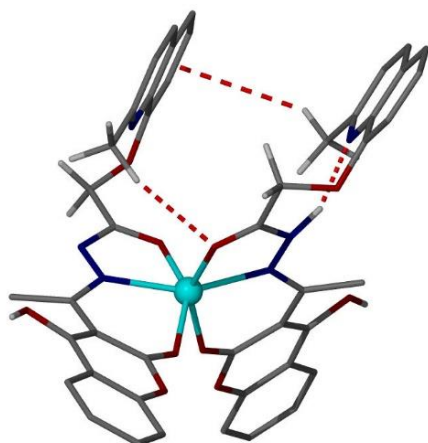


Fig 7. DFT fully optimized structure of *syn*-[Zn(QHC2)₂].

Cell Studies

There have many studies that suggest Zn²⁺ ions play pivotal roles in human neurophysiology.⁴⁹ Moreover, zinc pathology is important as many biological systems require that zinc homeostasis is maintained under physiological conditions.⁵⁰ Both increasing and decreasing zinc concentrations can have a detrimental effect on the function of the cell. For example, the lack of zinc in the kidney cells has been linked to kidney disease. Therefore, monitoring biologically relevant metal ions is of interest. The other “silent” metal of interest is Cd²⁺ ions. Cadmium²⁺ has no known biological use and bioaccumulation of Cd²⁺ ions has significant consequences.⁵¹ Cadmium has been ranked as one of the top 10 priority lists from the top 275 hazardous materials that have been identified by The

Comprehensive Environmental Response, Compensation, and Liability Act in the USA⁵², therefore, detection and remediation of Cd²⁺ ions in the cell are imperative. Once it enters the body, approximately 40% of the cadmium will accumulate in the kidneys, which can trigger acute kidney injury (AKI). Increased concentration of Cd²⁺ ions also destroys the lysosomal function, leading to cell death and kidney failure.

To understand the performance and biocompatibility of the QHC1 and QHC2 sensors, trials were conducted in Human embryonic kidney (HEK) cells (obtained from the American Type Culture Collection-ATCC-and grown under standard conditions outlined in the ESI). First a cell viability assay was performed based on detection of lactate dehydrogenase (LDH) in culture media to quantify cell lysis. The cells were grown under standard conditions (see supporting information). Five concentrations of QHC1 and QHC2 (500 ng·mL⁻¹, 2.5, 5, 25 and 50 μg·mL⁻¹) were incubated with the cells for 24 h, after which cell-free media was collected to assess LDH activity. Detection was through a colorimetric/absorbance measure of a water-soluble tetrazolium salt that when reduced by NADH is converted to red formazan that is seen at 490 nm. The product of the assay is a consequence of LDH generating NADH by reducing NAD⁺ from converting lactate to pyruvate. The data collected are based on two values: one that represents zero-cytotoxicity (background) and the other 100% cytotoxicity. The plot of 100% viability against the concentration is shown in Fig. 8. Overall, the QHC1 sensor was well-tolerated by the cells, with only the highest concentration showing compromised viability that was significantly different. Even at its highest concentration QHC1 showed a less than 30% reduction in viability. In contrast QHC2 had a greater impact on viability where even at the lowest concentrations, greater than 20% loss of viability was seen. The cause of this difference is unclear but may be due to alternate interactions with cell components by the QHC2 methyl group.

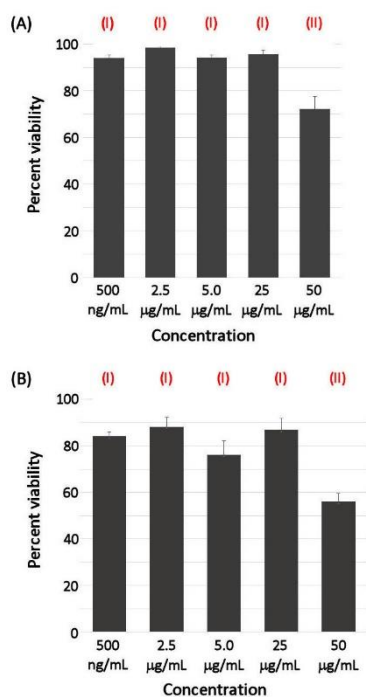


Fig 8. HEK293 viability determined by LDH assay. (A) is percent cell viability after treatment with **QHC1** and (B) with **QHC2**. All experiments were run in triplicate. (I) designates four concentrations that are statistically identical with over 80% cell viability and (II) shows that the highest concentration (50 $\mu\text{g}\cdot\text{mL}^{-1}$) used for both dyes were statistically distinct from other concentrations as determined by Tukey ANOVA.

Following assessment of viability, subcellular distribution was characterized using the 25 $\mu\text{g}\cdot\text{mL}^{-1}$ concentration. Cells were imaged using a Stellaris STED confocal microscope with a 405

nm excitation. Emission spectra were collected between 420–500 nm. PMT images were also collected to reveal cell morphology. Further as part of this test ZnCl_2 and CdCl_2 ions were added to reveal differences in distribution. These tests revealed greater brightness when the metal ions were added, which is consistent with sensor behavior in *ex vivo* assays, Fig 9. Moreover, the brightness intensity of **QHC1** and **QHC2** dyes within live HEK293 cells, both in the presence and absence of metal ions. Strikingly, the results conclusively reveal a substantial increase in brightness when closed shell metal ions are introduced to the cellular environment, Fig 10. This observation carries exceptional significance as it underscores the role of metal ions as potent enhancers of the fluorescence properties of these dyes within the cellular milieu. The implications of this finding are particularly relevant in the realm of cellular imaging, where heightened brightness is a critical parameter for precision and accuracy.

Control experiments involving the addition of **QHC1** and **QHC2** ligands alone showed very little background fluorescence in the lysosomal/endosomal system (Figs. S58 and S61). This demonstrates that the observed fluorescence signal is due to the interaction of zinc and the probe as the lysosomal and endosomal organelles became significantly more pronounced (Figs. S59 and S62). This phenomena also occurs in cancer cell lines.⁵³ Interestingly, Cd^{2+} ion addition led to a highly distinct distribution (Figs. S60 and S62). Unlike after Zn^{2+} addition, diffuse staining could be observed throughout the cell with some weaker fluorescence even seen in the nucleus. This suggests that both molecules are membrane permeable, which is consistent with their small size (m for **QHC1** = 403 Da and **QHC2** = 417 Da). A punctate distribution of **QHC1** and **QHC2** was observed, suggesting that the free zinc is in membrane-bound organelles not in the cytoplasm. As lysosomes have been shown

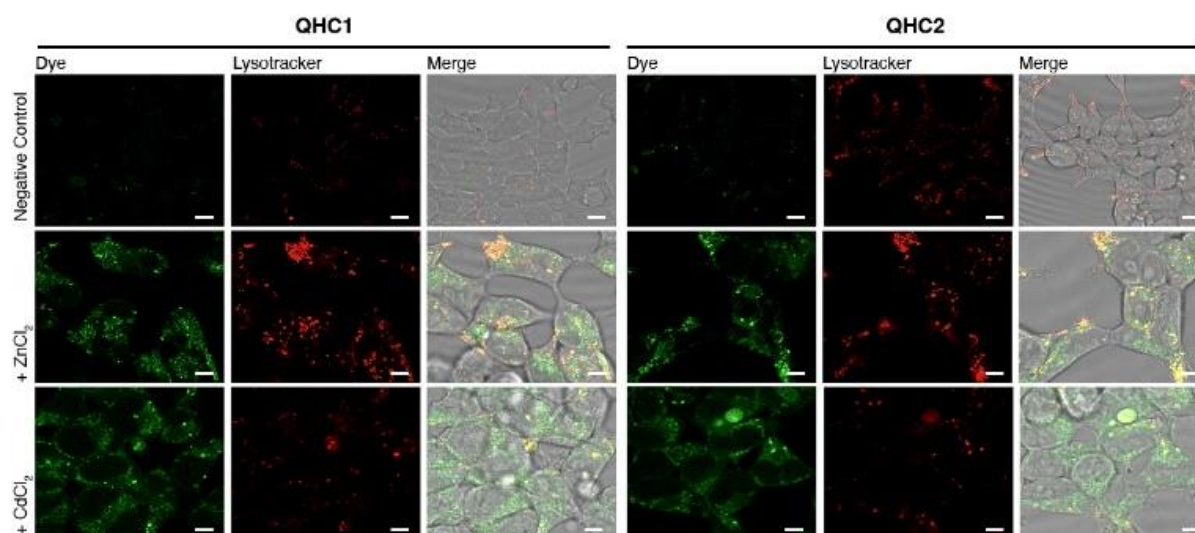


Fig. 9: Brightness intensity of **QHC1** and **QHC2** (2.5 $\mu\text{g}\cdot\text{mL}^{-1}$) with and without ZnCl_2 (10 $\mu\text{mol}\cdot\text{dm}^{-3}$) or CdCl_2 (10 $\mu\text{mol}\cdot\text{dm}^{-3}$) in live HEK293 cells. Top row: a minimal signal is seen in lysosomes for **QHC2** in cells loaded with probes alone. Middle row: dye fluorescence after addition of ZnCl_2 showing that **QHC1** accumulates in lysosomes while **QHC2** is more diffuse in the cytoplasm. Bottom row: dye fluorescence after addition CdCl_2 in which both probes are significantly localized in the cytoplasm with some accumulation in lysosomes. Scale bar = 5 μm .

to concentrate Zn^{2+} ions it is reasonable to suggest that dissociation of the Zn^{2+} ions from the molecular probes can occur in the cytoplasm and the dissociated zinc is taken up by the lysosomes. The Cd^{2+} ions become more widely distributed in cells compared to Zn^{2+} , which may be related to the cell possessing specific Zn^{2+} carrier mechanisms that are not present for Cd^{2+} ions. To understand the distinctive trafficking behavior of dyes in response to metal ions, we conducted colocalization experiments following an overnight incubation with HEK293 cells. We employed LysoTracker deep red to label lysosomes and quantified the colocalization of **QHC1**, **QHC2** (in the presence of $ZnCl_2$ and $CdCl_2$), and LysoTracker (Fig. 11). As anticipated, the colocalization of the dyes with LysoTracker was significantly elevated in cells treated with $ZnCl_2$, yielding a Pearson's Correlation Coefficient of approximately 0.7, in contrast to cells treated with $CdCl_2$, which yielded a Pearson's Correlation Coefficient of around 0.57 (Fig 11). These findings provide additional empirical support for the hypothesis that the dyes tend to diffuse more extensively into the cytoplasm following incubation with $CdCl_2$, whereas $ZnCl_2$ tends to be preferentially sequestered by the lysosomes.

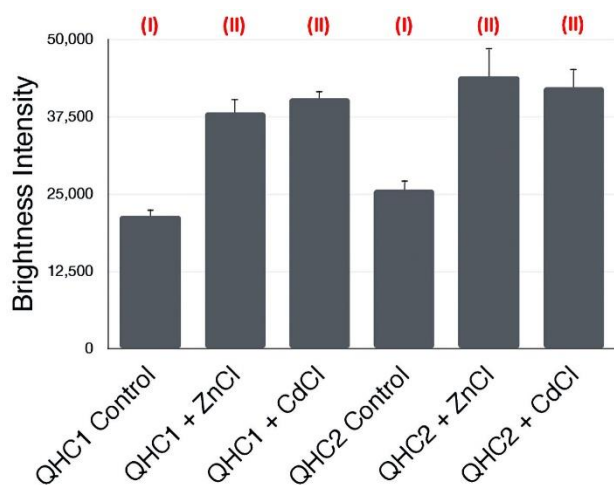


Fig. 10. Brightness intensity of **QHC1** and **QHC2** with and without metal ions in live HEK293 cells. These tests revealed greater brightness when metal ions were added to the dyes. The Tukey ANOVA statistical method was applied to the dataset.

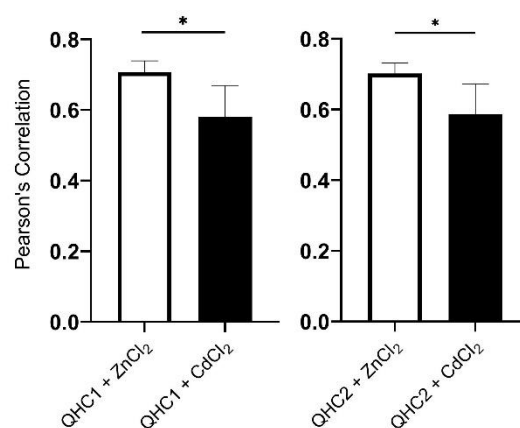


Fig. 11 Pearson's correlation graphs illustrating the colocalization relationship of **QHC1** and **QHC2** in lysosomes following treatment with $ZnCl_2$ or $CdCl_2$. LHS graph pertains to **QHC1**, while RHS graph relates to **QHC2**. As expected, it was observed a substantial increase in colocalization between the dyes and LysoTracker when treated with $ZnCl_2$ compared to cells treated with $CdCl_2$. The statistical analysis was conducted using the pairwise T-test.

Conclusion

In summary, two structurally similar molecular chemodosimeters have been synthesized in four-steps in respectable yields, and both have been shown to bind Zn^{2+} and Cd^{2+} ions effectively. Solution speciation is dependent on the presence or absence of a methyl group on the quinoline moiety and the counterion used. The binding affinities were determined by UV-Vis and steady-state fluorescence and the optical changes are a consequence of excimer formation of the quinoline groups. Despite the molecular probe having a functional group that can undergoes ESIP this phenomenon was not observed in the steady-state fluorescence but was shown to exist in the fluorescence decay experiments. Moreover, the NMR investigation only showed one geometrical isomer. Molecular modelling calculations suggested a number of possible coordination complexes could exist in solution and support the existence of various fluorescent species. Finally, both molecular probes can permeate the HEK293 cell membrane to monitor both Zn^{2+} and Cd^{2+} ions.

Author contributions

Conceptualization: A.A, H.B.J and K.J.W. The synthesis of the compounds used in this studied were carried out by the Tunisian team (A.A and B.B), led by H.B.J. The photophysical studies were carried out at Southern Miss by M.M.S and R.M. Molecular modelling (P.J.C) and the cell work was conducted A.F, I.O. and M.H. All of the authors contributed to the data analysis presented in the manuscript and supporting information. K.J.W was responsible for drafting the manuscript and the overall management of this international collaboration. Review and editing of the final draft were carried out by A.A, H.B.J, M.M.S. R.M., P.J.C and K.J.W.

Conflicts of Interest

There are no conflicts of interest to declare as part of this work.

Acknowledgments

K.J.W would like to thank the Department of the Army US Army Engineer Research and Development Centre ERDC (Contract W912HZ-19-2-0044). A.F. would like to thank NSF award 1757220, CBET MRI 2019023 and the Mississippi INBRE P20GM103476 and H.B.J. thanks the Ministry of Higher Education and Scientific Research of Tunisia for the financial support to the LR11ES39 laboratory.

Notes and references

† Supporting information contains experimental data, steady-state optical studies, modelling and lifetime data.

1. K. J. Wallace, A. D. G. Johnson, W. S. Jones and E. Manandhar, *Chemodosimeters and chemoreactands for sensing ferric ions*, *Supramol. Chem.*, 2018, **30**, 353-383.
2. D. T. Quang and J. S. Kim, Fluoro- and chromogenic chemodosimeters for heavy metal ion detection in solution and biospecimens, *Chem. Rev.*, 2010, **110**, 6280-6301.
3. Y. Yang, C.-Y. Gao, J. Chen, N. Zhang and D. Dong, A pyrene-based fluorescent and colorimetric chemodosimeter for the detection of ClO⁻ ions, *Anal. Methods*, 2016, **8**, 805-809.
4. T. Liu, J. Hu, J. Yin, Y. Zhang, C. Li and S. Liu, Enhancing detection sensitivity of responsive microgel-based Cu(II) chemosensors via thermo-induced volume phase transitions, *Chem. Mater.*, 2009, **21**, 3439-3446.
5. H. Liu, Y. Tan, Q. Dai, H. Liang, J. Song, J. Qu and W.-Y. Wong, A simple amide fluorescent sensor based on quinoline for selective and sensitive recognition of zinc(II) ions and bioimaging in living cells, *Dyes and Pigments*, 2018, **158**, 312-318.
6. A. Panja and K. Ghosh, Triazole-amide isosteric pyridine-based supramolecular gelators in metal ion and biothiol sensing with excellent performance in adsorption of heavy metal ions and picric acid from water, *New J. Chem.*, 2019, **43**, 934-945.
7. Z. Xu, K.-H. Baek, H. N. Kim, J. Cui, X. Qian, D. R. Spring, I. Shin and J. Yoon, Zn²⁺-Triggered amide tautomerization produces a highly Zn²⁺-selective, cell-permeable, and ratiometric fluorescent sensor, *J. Am. Chem. Soc.*, 2010, **132**, 601-610.
8. F.-U. Rahman, A. Ali, S. K. Khalil, R. Guo, P. Zhang, H. Wang, Z.-T. Li and D.-W. Zhang, Tuning sensitivity of a simple hydrazone for selective fluorescent "turn on" chemo-sensing of Al³⁺ and its application in living cells imaging, *Talanta*, 2017, **164**, 307-313.
9. A. Subhasri, S. Balachandran, K. Mohanraj, P. S. Kumar, K. J. Jothi and C. Anbuselvan, Synthesis, Computational and cytotoxicity studies of aryl hydrazones of β-diketones: Selective Ni²⁺ metal Responsive fluorescent chemosensors, *Chemosphere*, 2022, **297**, 134150.
10. A. B. Davis, M. H. Ihde, A. M. Busenlehner, D. L. Davis, R. Mia, J. Panella, F. R. Fronczek, M. Bonizzoni and K. J. Wallace, Structural features of a family of coumarin-enamine fluorescent chemodosimeters for ion pairs, *Inorg. Chem.*, 2021, **60**, 14238-14252.
11. H. S. Kumbhar, U. N. Yadav, B. L. Gadilohar and G. S. Shankarling, A highly selective fluorescent chemosensor based on thio-β-enaminone analog with a turn-on response for Cu(II) in aqueous media, *Sensors and Actuators B: Chemical*, 2014, **203**, 174-180.
12. L. Tang, S. Ding and X. Yan, A 2-(2'-hydroxyphenyl)quinazolin-4(3H)-one derived enaminone for fluorescence detection of Pd²⁺, *Inorganic Chemistry Communications*, 2016, **74**, 35-38.
13. R. Kumar, P. Gahlyan, N. Yadav, M. Bhandari, R. Kakkar, M. Dalela and A. K. Prasad, Bis-triazolylated-1,4-dihydropyridine - Highly selective hydrophilic fluorescent probe for detection of Fe³⁺, *Dyes and Pigments*, 2017, **147**, 420-428.
14. X. Zhou, P. Li, Z. Shi, X. Tang, C. Chen and W. Liu, A highly selective fluorescent sensor for distinguishing cadmium from zinc ions based on a quinoline platform, *Inorg. Chem.*, 2012, **51**, 9226-9231.
15. S. Chekir, M. Debbabi, A. Regazzetti, D. Dargère, O. Laprèvote, H. B. Jannet and R. Gharbi, Design, synthesis and biological evaluation of novel 1, 2, 3-triazole linked coumarinopyrazole conjugates as potent anticholinesterase, anti-5-lipoxygenase, anti-tyrosinase and anti-cancer agents, *Bioorg. Chem.*, 2018, **80**, 189-194.
16. U. Saha, S. Mabhai, B. Das, G. S. Kumar, P. Brandão and M. Dolai, Combined theoretical and experimental investigation of a DNA interactive poly-hydroxyl enamine tautomer exhibiting "turn on" sensing for Zn²⁺ in pseudo-aqueous medium, *New J. Chem.*, 2021, **45**, 20806-20817.
17. F. Wang, K. Wang, Q. Kong, J. Wang, D. Xi, B. Gu, S. Lu, T. Wei and X. Chen, Recent studies focusing on the development of fluorescence probes for zinc ion, *Coordination Chemistry Reviews*, 2021, **429**, 213636.
18. S. Qu, Q. Cao, J. Ma and Q. Jia, A turn-on fluorescence sensor for creatinine based on the quinoline-modified metal organic frameworks, *Talanta*, 2020, **219**, 121280.
19. B. Zhang, H. Liu, F. Wu, G. Hao, Y. Chen, C. Tan, Y. Tan and Y. Jiang, A dual-response quinoline-based fluorescent sensor for the detection of Copper (II) and Iron(III) ions in aqueous medium, *Sensors and Actuators B: Chemical*, 2017, **243**, 765-774.
20. Y. Liu, X. Qu, Q. Guo, Q. Sun and X. Huang, QD-Biopolymer-TSP assembly as efficient BIFRET sensor for ratiometric and visual detection of zinc ion, *ACS Appl. Mater. Interfaces*, 2017, **9**, 4725-4732.
21. S. Sakunkaewkasem, A. Petdum, W. Panchan, J. Sirirak, A. Charoenpanich, T. Sooksimuang and N. Wanichacheva, Dual-Analyte Fluorescent Sensor Based on [5]Helicene Derivative with Super Large Stokes Shift for the Selective Determinations of Cu²⁺ or Zn²⁺ in Buffer Solutions and Its Application in a Living Cell, *ACS Sensors*, 2018, **3**, 1016-1023.
22. M. Schrag, A. Crofton, M. Zabel, A. Jiffry, D. Kirsch, A. Dickson, X. W. Mao, H. V. Vinters, D. W. Domaille, C. J. Chang and W. Kirsch, Effect of cerebral amyloid angiopathy on brain iron, copper, and zinc in Alzheimer's disease, *J. Alzheimer's Dis.*, 2011, **24**, 137-149.
23. A. Fallah, A. Mohammad-Hasani and A. H. Colagar, Zinc is an Essential Element for Male Fertility: A Review of Zn Roles in Men's Health, Germination, Sperm Quality, and Fertilization, *J Reprod Infertil*, 2018, **19**, 69-81.
24. S.-H. Choi, K.-L. Lee, J.-H. Shin, Y.-B. Cho, S.-S. Cha and J.-H. Roe, Zinc-dependent regulation of zinc import and export genes by Zur, *Nat Commun*, 2017, **8**, 15812.
25. W. Maret, Zinc in cellular regulation: The nature and significance of "Zinc signals", *Int. J. Mol. Sci.*, 2017, **18**, 2285.
26. L. Mezzaroba, D. F. Alfieri, A. N. C. Simão and E. M. V. Reiche, The role of zinc, copper, manganese and iron in neurodegenerative diseases, *Neurotoxicology*, 2019, **74**, 230-241.

- 27 J. Jansen, W. Karges and L. Rink, Zinc and diabetes—clinical links and molecular mechanisms, *J. Nutr. Biochem.*, 2009, **20**, 399-417.
- 28 U. Doboszewska, K. Młyniec, A. Właż, E. Poleszak, G. Nowak and P. Właż, Zinc signaling and epilepsy, *Pharmacol. Ther.*, 2019, **193**, 156-177.
- 29 Z. Qi and K. J. Liu, The interaction of zinc and the blood-brain barrier under physiological and ischemic conditions, *Toxicol. Appl. Pharmacol.*, 2019, **364**, 114-119.
- 30 W. Maret, in *Zinc Signals in Cellular Functions and Disorders*, eds. T. Fukada and T. Kambe, Springer Japan, Tokyo, 2014, pp. 7-26.
- 31 E. M. Nolan and S. J. Lippard, The zinspy family of fluorescent zinc sensors: syntheses and spectroscopic investigations, *Inorg. Chem.*, 2004, **43**, 8310-8317.
- 32 E. M. Nolan, J. W. Ryu, J. Jaworski, R. P. Feazell, M. Sheng and S. J. Lippard, Zinspy sensors with enhanced dynamic range for imaging neuronal cell zinc uptake and mobilization, *J. Am. Chem. Soc.*, 2006, **128**, 15517-15528.
- 33 H. Irving and R. J. P. Williams, The stability of transition-metal complexes, *J. Chem. Soc.*, 1953, 3192-3210.
- 34 R. A. Colvin, W. R. Holmes, C. P. Fontaine and W. Maret, Cytosolic zinc buffering and muffling: Their role in intracellular zinc homeostasis, *Metallomics*, 2010, **2**, 306-317.
- 35 C. Wolf, A. Weth, S. Walcher, C. Lax and W. Baumgartner, Modeling of Zinc Dynamics in the Synaptic Cleft: Implications for Cadherin Mediated Adhesion and Synaptic Plasticity, *Front Mol Neurosci*, 2018, **11**, 306.
- 36 A. B. Davis, R. E. Lambert, F. R. Fronczek, P. J. Cragg and K. J. Wallace, An activated coumarin-enamine Michael acceptor for CN⁻, *New J. Chem.*, 2014, **38**, 4678-4683.
- 37 R. Munir, N. Javid, M. Zia-ur-Rehman, M. Zaheer, R. Huma, A. Roohi and M. M. Athar, Synthesis of novel N-acylhydrazones and their CN/NN bond conformational characterization by NMR spectroscopy, *Molecules*, 2021, **26**, 4908.
- 38 M. Horchani, G. Della Sala, A. Caso, F. D'Aria, G. Esposito, I. Laurenzana, C. Giancola, V. Costantino, H. B. Jannet and A. Romdhane, Molecular docking and biophysical studies for antiproliferative assessment of synthetic pyrazolo-pyrimidinones tethered with hydrazide-hydrazones, *Int. J. Mol. Sci.*, 2021, **22**, 2742.
- 39 D. Venkataraman, Y. Du, S. R. Wilson, K. A. Hirsch, P. Zhang and J. S. Moore, A coordination geometry table of the d-block elements and their ions, *J. Chem. Educ.*, 1997, **74**, 915.
- 40 A. Mallet, A. B. Davis, D. Davis, J. Panella, K. J. Wallace and M. Bonizzoni, A cross reactive sensor array to probe divalent metal ions, *Chem. Commun.*, 2015, **51**, 16948-16951.
- 41 E. Manandhar and K. J. Wallace, Host-guest chemistry of pyrene-based molecular receptors, *Inorg. Chim. Acta*, 2012, **381**, 15-43.
- 42 L. Naik and N. Math, Photo physical properties of 8-hydroxy quinoline, *Indian J. Pure Appl. Phys.*, 2005, **43**, 743-749.
- 43 J. J. Hurley, Q. J. Meisner, C. Huang and L. Zhu, Hydroxyaromatic fluorophores, *ACS Omega*, 2021, **6**, 3447-3462.
- 44 M. Itoh and Y. Fujiwara, Transient absorption and two-step laser excitation fluorescence studies of photoisomerization in 2-(2-hydroxyphenyl) benzoxazole and 2-(2-hydroxyphenyl) benzothiazole, *J. Am. Chem. Soc.*, 1985, **107**, 1561-1565.
- 45 H. C. Joshi and L. Antonov, Excited-state intramolecular proton transfer: A short introductory review, *Molecules*, 2021, **26**, 1475.
- 46 E. Tervola, K.-N. Truong, J. S. Ward, A. Priimagi and K. Rissanen, Fluorescence enhancement of quinolines by protonation, *RSC advances*, 2020, **10**, 29385-29393.
- 47 L. Jamalzadeh, H. Ghafoori, R. Sariri, H. Rabuti, J. Nasirzade, H. Hasani and M. R. Aghamaali, Cytotoxic effects of some common organic solvents on MCF-7, RAW-264.7 and human umbilical vein endothelial cells, *Avicenna J Med Biochem.*, 2016, **4**, e33453.
- 48 K. Berend, L. H. Van Hulsteijn and R. O. Gans, Chloride: the queen of electrolytes?, *Eur. J. Intern. Med.*, 2012, **23**, 203-211.
- 49 S. Choi, D. K. Hong, B. Y. Choi and S. W. Suh, Zinc in the brain: friend or foe?, *Int. J. Mol. Sci.*, 2020, **21**, 8941.
- 50 M. Murakami and T. Hirano, Intracellular zinc homeostasis and zinc signaling, *Cancer Sci.*, 2008, **99**, 1515-1522.
- 51 H. Zhang and M. Reynolds, Cadmium exposure in living organisms: A short review, *Sci. Total Environ.*, 2019, **678**, 761-767.
- 52 J. R. MacAyeal, The comprehensive environmental response, compensation, and liability act: The correct paradigm of strict liability and the problem of individual causation, *J. Environ. Law*, 1999, **18**, 217-334.
- 53 A. R. Cowley, J. Davis, J. R. Dilworth, P. S. Donnelly, R. Dobson, A. Nightingale, J. M. Peach, B. Shore, D. Kerr and L. Seymour, Fluorescence studies of the intra-cellular distribution of zinc bis (thiosemicarbazone) complexes in human cancer cells, *Chem. Commun.*, 2005, 845-847.